

## **Recycling mica and carbonate-rich mine tailings in alkali-activated composites: A synergy with metakaolin**

Niu He, Abdulkareem Mariam, Sreenivasan Harisankar, Kantola Anu M., Havukainen Jouni, Horttanainen Mika, Telkki Ville-Veikko, Kinnunen Paivo, Illikainen Mirja

This is a Final draft version of a publication  
published by Elsevier  
in Minerals Engineering

**DOI:** 10.1016/j.mineng.2020.106535

**Copyright of the original publication:** © 2020 Elsevier Ltd.

### **Please cite the publication as follows:**

Niu, H., Abdulkareem, M., Sreenivasan, H., Kantola, A M., Havukainen, J., Horttanainen, M., Telkki, V V., Kinnunen, P., Illikainen, M. (2020). Recycling mica and carbonate-rich mine tailings in alkali-activated composites: A synergy with metakaolin. Minerals Engineering, Vol 157, 106535. DOI: 10.1016/j.mineng.2020.106535

**This is a parallel published version of an original publication.  
This version can differ from the original published article.**

# Recycling mica and carbonate-rich mine tailings in alkali-activated composites: a synergy with metakaolin

He Niu <sup>a</sup>, Mariam Abdulkareem <sup>b</sup>, Harisankar Sreenivasan <sup>a</sup>, Anu M. Kantola <sup>c</sup>, Jouni Havukainen <sup>b</sup>,  
Mika Horttanainen <sup>b</sup>, Ville-Veikko Telkki <sup>c</sup>, Paivo Kinnunen <sup>a\*</sup>, Mirja Illikainen <sup>a</sup>

<sup>a</sup> Fibre and Particle Engineering Research Unit, University of Oulu, P.O. Box 4300, FI-90570, Oulu, Finland

<sup>b</sup> Lappeenranta-Lahti University of Technology, School of Energy Systems, Department of Sustainability Science,  
P.O.Box 20, FI-53851, Lappeenranta, Finland

<sup>c</sup> NMR Research Unit, Faculty of Science, University of Oulu, P.O. Box 3000, FI-90014 University of Oulu, Finland

## Abstract

The main objective of this paper was to investigate the alkali activation of mine tailings (MT) after mechanochemical activation and the effect of metakaolin (MK) addition. Finnish mica-rich tailings from a phosphate mine were studied as precursors for alkali-activated materials (AAM) with a potential application as a substitute for ordinary Portland cement (OPC). The principal physical properties (water absorption, apparent porosity and unconfined compressive strength) were measured for samples containing 30% to 70% tailings. Zeolite phases such as natrolite and cancrinite were observed and the formation of C-(N)-A-S-H<sup>1</sup> and N-A-S-H gels was identified by XRD, DRIFT, FESEM-EDS and NMR technologies. A life cycle assessment (LCA) was conducted on specimens in comparison to OPC. This work indicated that phosphate MT can be recycled through alkali activation with lower CO<sub>2</sub> emission compared to all-metakaolin geopolymers and that the binder phase formed at the most promising tailings contents (60% to 70%) was C-(N)-A-S-H gel.

Keywords: mine tailings; metakaolin; geopolymers; gel chemistry; life cycle assessment; zeolite; mechanochemical activation

## 1. Introduction

Greenhouse gas emissions are a global issue and the leading cause of the global climate change. One tonne of Portland cement manufactured produces approximately one tonne of carbon dioxide (Hasanbeigi et al., 2010). Therefore, developing materials with lower CO<sub>2</sub> emission as alternative to the traditional Portland cement is important. Alkali-activated materials (AAM) are cementitious binders that have been investigated for several decades with respect to their excellent performances and mechanical properties, refractory, and acid resistance (Bakharev, 2005; Duxson et al., 2007; Novais et al., 2018; Vickers et al., 2015). AAM can contribute to reduce the carbon footprint, especially when waste materials, such as fly ash, slag, waste rocks and mine tailings are utilised (Kinnunen et al., 2018; MacKenzie et al., 2007; Maragkos et al., 2009; Rattanasak and Chindaprasirt, 2009).

AAM are produced from solid precursors under alkaline conditions, which involves both a high-calcium system and low-calcium system (geopolymer), containing C-(A)-S-H gel and N-A-S-H gel, respectively (Provis, 2013). Moreover, the coexistence of both cementitious binder gels; that is, C-(N)-A-S-H is possible. (Yip et al., 2005) The compatibility of C-S-H and N-A-S-H systems has been found to be highly susceptible to the threshold value of OH<sup>-</sup> concentration, which also influences the gel formation sequences (S Alonso

<sup>1</sup> C-CaO, N-Na<sub>2</sub>O, A-Al<sub>2</sub>O<sub>3</sub>, S-SiO<sub>2</sub>, H-H<sub>2</sub>O

\* Corresponding author.

E-mail address: Paivo.Kinnunen@oulu.fi

41 and Palomo, 2001; Santiago Alonso and Palomo, 2001). Calcium addition has also been used to modify the  
42 N-A-S-H gels, forming (N,C)-A-S-H gels under high pH conditions (>12) (García-Lodeiro et al., 2010). The  
43 product phase of sodium-silicate activation of Ca-containing aluminosilicate precursors consists of  
44 amorphous C-A-S-H gel along with C-(N)-A-S-H gel (Myers et al., 2015).

45 MT are currently underutilised industrial side streams, with potential to be used as a secondary raw material  
46 in AAM. The usual disposal of phosphate MT is done by transporting them to storage impoundments  
47 (Kauppila et al., 2013). The storage of tailings poses an environmental risk and cost money and energy for  
48 construction and maintenance. Therefore, the reprocessing and remediation of mining waste is an interesting  
49 alternative. The Siilinjärvi phosphate MT (Eastern Finland) consists of 65% phlogopite mica (2:1-layer  
50 lattice aluminosilicate) in addition to carbonates, silicates and apatite (O'Brien et al., 2015). It cannot be  
51 directly used for alkali activation due to its poor chemical reactivity. Furthermore, the gel formation of MT-  
52 based geopolymer is a complex issue as it depends on the specific minerals presenting in the tailings and has  
53 been little explored so far. Since MT are not highly reactive precursors, they have been mostly used in  
54 conjunction with reactive raw materials, such as metallurgical slag. Thermal analysis was successfully  
55 conducted on the tailings-slag geopolymers, indicating both C-S-H and C-A-S-H gels decomposition and  
56 recrystallisation (J. Ye et al., 2014). Zhang et al. (Zhang, 2013) summarised that waste materials such as  
57 hematite tailings, gold MT, copper MT can be used for producing geopolymer bricks, among which the  
58 coexistence of CaCO<sub>3</sub> and N-A-S-H gel systems was achieved by introducing cement kiln dust for alkali  
59 activation (Ahmari and Zhang, 2013). These studies shed the light on the gel formation in tailings-based  
60 geopolymers and on how to guide the gel development in tailings-based geopolymers.

61 Pre-treatment is often necessary for MT before utilisation. S. Moukannaa et al. (Moukannaa et al., 2019,  
62 2018) studied the heat treatment and alkaline fusion on phosphate MT, and they also investigated the alkali  
63 activation of such pre-treated tailings with fly ash and MK. Although this study carried out the recycling of  
64 phosphate MT, the tailings consisted mainly of fluorapatite and quartz, and therefore the findings are not  
65 relevant to the utilisation of mica and carbonate-rich side streams. In addition, high-energy pre-treatments  
66 can be energy and time consuming compared to mechanochemical treatment, which is a more efficient and  
67 greener method (Boldyreva, 2013). Mechanochemical activation, especially intensive grinding, can generate  
68 internal stress, induced by shear force and impact between particles and grinding media. In our previous  
69 research, the amorphisation of phlogopite-bearing phosphate MT by mechanochemical activation was  
70 observed (Niu et al., 2020). Alkaline reactivity tests demonstrated that mechanochemical activation  
71 improved reactivity seen as increased silicon and aluminium dissolution rates in alkaline media.  
72 Mechanochemical activation has been conducted on different precursors, such as kaolin (Balczár et al.,  
73 2016), fly ash (Mucsi et al., 2015), natural minerals (MacKenzie et al., 2007) and vanadium MT (Wei et al.,  
74 2017) for the purpose of alkali activation; however, the effect of mechanochemical activation on phosphate  
75 MT has not been studied.

76 Therefore, the aim of this work was to alkali-activate phosphate MT with various tailings/MK mass ratios  
77 and to investigate the mechanism of gel formation in this complex multi-mineral system. Thus, it might be  
78 possible to guidance the utilization of mine tailings as secondary materials for construction and building  
79 application. Life cycle assessment of the end-products was conducted and compared to similar construction  
80 materials based on ordinary Portland cement (OPC).

## 81 2. Materials and methods

82 The metakaolin (MK; MetaMax, Aquaminerals Finland Ltd) was purchased from BASF (Germany) and the  
83 phosphate MT were obtained from Siilinjärvi phosphate mining site (yearly production:10 Mt/a; Stock:  
84 280 Mt), Finland, which mainly consists of phlogopite (64%), dolomite (6%), calcite (14%) and tremolite  
85 (1.4%). The chemical compositions of both MK and MT are provided in

86 Table 1. The sodium hydroxide (VWR Chemicals, >97%) and sodium silicate solution (VWR Chemicals,  
87 SiO<sub>2</sub>: 26.8%, Na<sub>2</sub>O: 8.2%) were used as alkali activator. Twelve M NaOH solution was prepared before  
88 experiments and left overnight to cool down.

89 The MT were subjected to mechanochemical activation (Vibratory disc mill; Retsch RS 200) before alkali-  
 90 activation according to our previous research. It indicated that 4-min ground raw tailings obtained a D50 of  
 91 7.22  $\mu\text{m}$  and a BET surface area of  $6.9745 \pm 0.0210 \text{ m}^2/\text{g}$ . In addition, it also generated around 40% of  
 92 amorphous phase according to Rietveld refinement. The X-ray diffraction and DRIFT were also conducted  
 93 on both precursors as provided in Figure A.1. The typical DRIFT bands of MK are shown in Figure A.1a,  
 94 after which Table 1 provides the positions and assigned bands of MT. It should be noted that the shift of  
 95 dolomite and calcite bands is significantly attributed to the pre-treatment and the Mg/Ca ratio in the initial  
 96 composition. For instance, the bands in the range of 2,600 to 2,500  $\text{cm}^{-1}$  can be assigned to the combination  
 97 of  $\nu_1$  and  $\nu_2$  modes, which is in line with the previous studies (Gunasekaran and Anbalagan, n.d.; Nguyen et  
 98 al., 1991). The morphologies of MK and mechanically activated MT are shown in Figure A.2 using scanning  
 99 electron microscope (FESEM, Zeiss). The particle shape of MT is normally irregular as MK.

100 *Table 1. Chemical composition of the raw materials by XRF analysis*

Sample	SiO <sub>2</sub>	Al <sub>2</sub> O <sub>3</sub>	CaO	MgO	K <sub>2</sub> O	Fe <sub>2</sub> O <sub>3</sub>	P <sub>2</sub> O <sub>5</sub>	TiO <sub>2</sub>	MnO	Others	L.O.I.
PMT	32.99	7.09	12.92	17.27	5.53	7.99	0.95	0.27	0.12	0.86	14.01
MK	53	44.5	-	-	0.1	0.4	-	1.4	-	-	0.3

101

## 102 2.1 Preparation of alkali-activated samples

103 The alkali-activation was subjected to the binary mixture of mechanochemically activated phosphate MT and  
 104 MK. The mix design is given in Table 2. The mass ratio of sodium silicate solution and sodium hydroxide  
 105 solution was fixed at 1.4 for all samples. The liquid to solid ratio was variable due to the rheological  
 106 properties of the slurry; however, the samples named through PM 3/7 to PM 7/3 had a constant liquid/solid  
 107 mass ratio of 0.35. Two precursors were dry-mixed for 5 min before alkali-activation. The slurry was  
 108 thoroughly blended by a high shear mixer at 1,000 rpm for 5 min; thereafter, it was shaped by using  
 109 Polyethylene moulds with dimensions of 20 mm in height and 25 mm in diameter. The vibrating machine  
 110 (Vortex-Genie 2, Prolab Oy) was used to remove all air bubbles. The samples were demoulded after curing  
 111 at 40 °C for 24 h and then continuously cured in a sealed plastic bag for 7 days.

112 *Table 2. Experimental mix design for alkali-activated materials\**

Sample name	PMT (Phosphate tailings)/wt%	MK (Metakaolin)/wt%	H <sub>2</sub> O/Na	Na/Al	Si/Al
PM 0/10	0	100	4.31	0.59	1.31
PM 1/9	10	90	4.29	0.65	1.39
PM 2/8	20	80	4.07	0.72	1.49
PM 3/7	30	70	3.70	0.8	1.62
PM 4/6	40	60	3.69	0.9	1.77
PM 5/5	50	50	3.67	1.03	1.97
PM 6/4	60	40	3.65	1.2	2.24
PM 7/3	70	30	3.64	1.44	2.60
PM 8/2	80	20	2.54	1.79	3.14
PM 9/1	90	10	2.53	2.37	4.03
PM 10/0	100	0	4.07	3.47	5.72

113 \* The calculated ratios are based on the assumption of fully reacted reactants.

## 114 2.2 Sample characterisation

115 Physical properties, such as apparent porosity and water absorption were tested according to the standard  
 116 EN-1936: 2006 (EN, 2007). After the preliminary UCS test of all the samples, subsequent characterisations  
 117 were conducted on five samples in particular through PM 3/7 to PM 7/3, since they were synthesised under  
 118 the same L/S ratio. The 7-day cured samples were crushed into pieces and mounted for scanning electron  
 119 microscopy (SEM). Apart from the SEM analysis, the fragments were ground manually using pestle and

120 mortar and submerged in isopropanol to remove the loosely bound water, thereby ceasing the alkali  
121 activation. The resulted powders were subsequently stored in a desiccator until measurement.

122 X-ray diffraction analysis was subjected to a Rigaku SmartLab 4.5 kW, with the equipment parameters of Co  
123 source (40 kV and 135 mA)  $K_{\alpha}$  ( $K_{\alpha 1}=1.78892 \text{ \AA}$ ;  $K_{\alpha 2}= 1.79278 \text{ \AA}$ ;  $K_{\alpha 1} /K_{\alpha 2}= 0.5$ ), scan rate of 3 °/min and  
124 0.02 °/step. The phase identification was conducted using the PDXL2 Software Suite with integrated PDF-4  
125 (2019) database. Chemical characterisation of hardened samples was performed by using diffuse reflectance  
126 infrared Fourier transform (DRIFT). The spectra were collected using a Bruker Vertex 80v spectrometer  
127 (USA) with a range of 400 to 4,000  $\text{cm}^{-1}$ , and 40 scans were taken at a resolution of 1  $\text{cm}^{-1}$  for each sample.  
128 The morphology of AAM was characterised with Zeiss ULTRA plus FESEM, with an acceleration voltage  
129 of 5 kV. FESEM-EDS (Energy Dispersive X-ray Spectroscopy) analysis was conducted using FESEM with  
130 an acceleration voltage of 15 kV and beam current of  $120 \times 10^{-8}$  A. The polished cross-sections of PM  
131 samples were subjected to at least 50 points analysis under the magnification of  $\times 3000$  and the working  
132 distance was 6 to 8 mm. UCS was performed with the Zwick Roell 100kN machine with a loading force of 3  
133 mm/min until failure. Soaking tests were performed by immersing three hardened samples in deionised water  
134 (DI-water) for 24 h with a sample/water mass ratio of 1/3 for each batch, after which the liquid and the solid  
135 were subjected to the inductively coupled plasma-optical emission spectroscopy (ICP-OES) and UCS,  
136 respectively.

137 The  $^{27}\text{Al}$  and  $^{29}\text{Si}$  NMR spectra were obtained on a Bruker Advance III 300 spectrometer operating at 78.24  
138 MHz for  $^{27}\text{Al}$  and 59.65 MHz for  $^{29}\text{Si}$ . For the purpose of conducting MAS experiments, the samples were  
139 packed into 7 mm zirconia rotors, then rotated with a frequency of 7 kHz. For  $^{27}\text{Al}$ , 2,048 scans were  
140 accumulated with a repetition rate of 2 s, and for  $^{29}\text{Si}$  the corresponding parameters were 8,192 scans and 3 s.  
141 Neither proton decoupling nor cross polarisation was used. The chemical shifts were referenced to  $\text{Al}(\text{NO}_3)_3$   
142 and TMS (tetramethylsilane), for which the reference shifts were set to zero ppm.

### 143 2.3 Life cycle assessment (LCA)

144 LCA is a method for assessing and evaluating potential environmental impacts of a product or system. It is  
145 performed in four phases: (1) goal and scope definition, (2) inventory phase, (3) impact assessment phase,  
146 and (4) interpretation phase (EN ISO 14040, 2006). This method has been applied in assessing the  
147 environmental impacts of numerous materials, including AAM (Abdulkareem et al., 2019; Passuello et al.,  
148 2017; Petrillo et al., 2016). The goal of the study is to estimate and compare impacts generated from  
149 developing alkali-activated binder from phosphate MT and MK in comparison to OPC. The study framework  
150 considers the four processes of cradle-to-gate alkali-activated binder formulations, including raw material  
151 production, waste beneficiation, mixing of constituents and associated emissions and energy consumptions.  
152 The functional unit is the production of 1 kg of binder. Excluded processes from this study include  
153 transportation as it is assumed all raw materials considered in this study are locally produced and have  
154 similar transportation distances. The use phase and end-of-life phase are also excluded from this study as it is  
155 assumed that comparable and similar impacts are expected from these phases.

156 The LCA study was performed using the Centrum voor Milieukunde Leiden (CML) 2016 method  
157 (Thinkstep, 2019). CML 2016 indicators provide information on the environmental issues associated with  
158 inputs and outputs of the product system (EN ISO 14040, 2006). This assessment principally focuses on  
159 global warming potential (GWP), acidification potential (AP), eutrophication potential (EP) and abiotic  
160 depletion potential (ADP fossil) impact categories. These impact categories are relevant for assessment of  
161 emissions generated during the production of binders (C. Chen et al., 2010; Van Den Heede and De Belie,  
162 2012), which is the central issue of this study. Moreover, the characterisation method for these impacts are  
163 better established than for the toxicity impacts, where both lack of reliable data and methodological  
164 uncertainty reduce their reliability (Merrild et al., 2012). The LCA modelling was performed using the GaBi  
165 LCA modelling software (version 8.6.0.20).

## 166 2.4 life cycle inventory

167 Life cycle inventory (LCI) is the phase where all unit processes included in the system boundary are  
168 quantified. LCI data of the different processes considered in this study are listed in Appendix B. Data sources  
169 for Life cycle inventory

170

171 Table B.1. The data were collected from GaBi database, scientific literature and environmental reports from  
172 industrial organisations. Unit processes such as sodium hydroxide, water and electricity were sourced from  
173 the GaBi database. The unit process of sodium silicate solution was modelled following the approach and  
174 LCI data from (Fawer et al., 1999). This solution is produced by dissolving sodium silicate lumps in water at  
175 an elevated temperature and pressure to yield a solution with 37% of total solids which is thereafter filtered  
176 (Fawer et al., 1999). Data for energy production were adapted to the Finnish context, and geographical scope  
177 of this study was limited to Finland, thus, a Finnish dataset was used. Where dataset for Finland is  
178 unavailable, the EU-28 dataset was used. For the baseline study, CEM I as reported by (CEMBUREAU,  
179 2015) was used as a basis of comparison. It composed about 92.5% clinker as main constituent and minor  
180 additional constituents. Environmental impacts of capital goods such as trucks, equipment, buildings were  
181 not taken into account in this study.

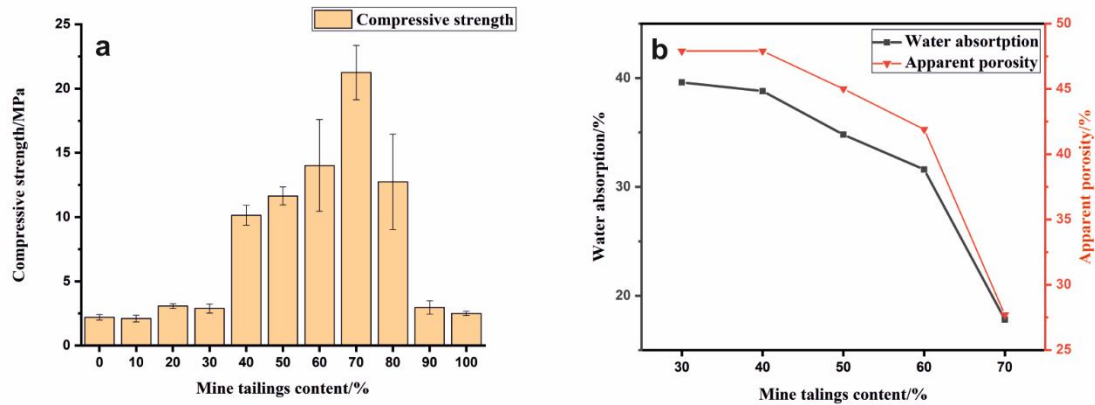
182 Oven curing is required for alkali-activated binder during production is essential for initiating chemical  
183 reaction of the binder at first instance. The energy consumed during curing in the lab was 1.87 MJ/kg at 40°C  
184 for 24 h. Mixing of the ingredients consumed 0.0045 MJ/kg and grinding of phosphate tailings consumed  
185 1.25 MJ/kg in the lab. Kaolin as reported from the GaBi database was already dried and milled. However, to  
186 produce metakaolin, kaolin had to be calcined, consuming 2.5 MJ/kg of natural gas (Heath et al., 2014; NLK,  
187 2002). The synthesis conditions for the alkali-activated binders are defined at laboratory scale. Thus, energy  
188 consumption is lower when full scale commercially tested technology is used.

## 189 3. Results and discussion

### 190 3.1 Physical properties

191 The 7-day UCS of alkali-activated binders are shown in Figure 1a. The variation of MK amount had a  
192 profound impact on the mechanical properties of tailings-metakaolin based geopolymers. It should be noted  
193 that the mix design here is not optimal for the alkali-activation of MK, thereby the solely MK-based  
194 geopolymer obtained a rather low UCS. With lower amounts of substitution of MK by MT from 0% to 30%,  
195 the UCS of each sample does not change considerably. When the proportion of MT continuously increases,  
196 the growth of UCS can be seen until it reaches 70%, at which point it gains the highest UCS of more than 20  
197 MPa. Thereafter, the UCS diminishes with the incremental MT content. The mix design of samples  
198 containing 30% to 70% MT was otherwise identical; therefore, the following characterisations were  
199 conducted on these specimens. The samples were specially dubbed as 'PM samples' in the following part of  
200 this article. Figure 1b demonstrates the variation of PM samples for water absorption and apparent porosity.  
201 It is obvious that apparent porosity and water absorption substantially decreased from PM 6/4 to PM 7/3,  
202 indicating the formation of highly dense binder regarding to the Si/Al ratio close to 2.6. The apparent  
203 porosity has a good correlation with their strength results; that is, the increasing UCS varies with decreasing  
204 apparent porosity and water absorption.



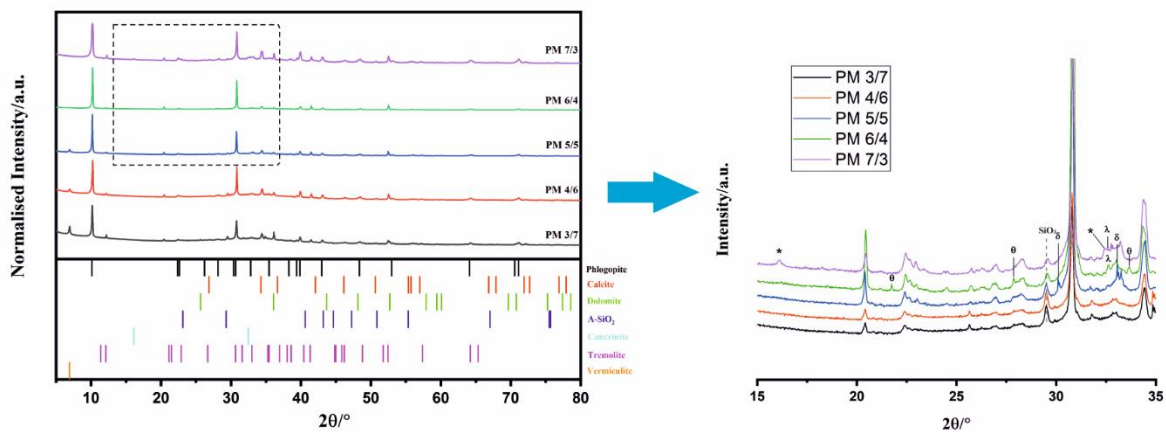


205

206 *Figure 1. a) Compressive strength of tailings-metakaolin based geopolymers after 7 days of curing, b) water absorption*  
 207 *and apparent porosity of tailings-metakaolin based geopolymers after 7 days of curing.*

208 3.2 XRD and DRIFT

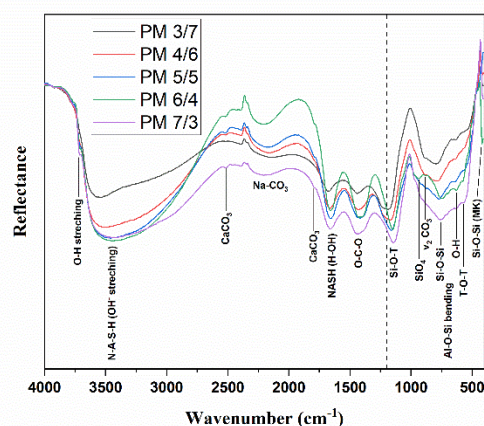
209 The diffractograms of PM samples are presented in Figure 2, in which XRD intensity was normalised by the  
 210 strongest reflections of each sample in order to compare the relative intensities. The main crystalline phases  
 211 of PM samples originate from MT, of which the mineralogical components include phlogopite (ICDD, PDF-  
 212 4 #04-012-5381), calcite (ICDD, PDF-4 #04-012-0489), dolomite (ICDD, PDF-4 #04-015-9848), and  
 213 tremolite (ICDD, PDF-4 #04-013-2249). A new phase conspicuously appeared in PM 3/7, PM 4/6 and PM  
 214 5/5 according to XRD pattern, which is ascribed to the reflection of vermiculite (ICDD, PDF-4 #04-017-  
 215 7291). Vermiculite is structurally analogous to phlogopite and has both balanced cations ( $Mg^{2+}$ ,  $Ca^{2+}$  and  
 216  $Na^+$ ) and water filling its interlayer. It should be mentioned that the  $K^+$  becomes loosely bonded in the  
 217 interlayer during mechanochemical activation. Thus, this transformation results from the cation exchange by  
 218 smaller  $Na^+$  during the alkali activation. The peak of  $SiO_2$  at around  $29^\circ/2\theta$  corresponds to the trend of  
 219 decreasing amount of raw metakaolin from PM 3/7 to PM 7/3. A new carbonate mineral, gaylussite, was  
 220 formed by reacting MT (containing intermediate calcium of 14.75%) with alkali activator in PM 5/5. As for  
 221 PM 6/4, a crystalline zeolite, natrolite, appeared alkali activation. Another crystalline phase, cancrinite,  
 222 shows in the XRD pattern of PM 7/3, nucleating from gels and acting as the microaggregates embedded in  
 223 the binder matrix (N. Ye et al., 2014).



224

225 *Figure 2. X-ray diffraction patterns of tailings-metakaolin based geopolymer samples.  $\delta$ : gaylussite (PDF# 04-010-3621);*  
 226  *$\theta$ : natrolite (PDF#04-011-7181);  $\lambda$ : sodium calcium carbonate (PDF#04-02102551); \*: cancrinite (PDF#04-015-*  
 227 *7815)*

228 Figure 3 shows DRIFT spectra of tailings-metakaolin based geopolymers, in which the band alternations  
 229 prove the occurrence of geopolymerisation. The partial disappearance of in-plane vibration in Al-O-Si band  
 230 at  $665\text{ cm}^{-1}$  (see Table A.1) indicates the decomposition of tetrahedral layers in amorphous phlogopite and  
 231 suggested that mechanochemical activated MT participated in the alkali activation. In addition, the weakened  
 232 band at  $720\text{ cm}^{-1}$  of MK during alkali activation is assigned to symmetric Al-O-Si stretching vibration (Mo et  
 233 al., 2014). The frequency at  $780\text{ to }790\text{ cm}^{-1}$  appearing demonstrated the unreacted  $\text{SiO}_2$  in the original MK  
 234 (Fernández-Jiménez and Palomo, 2005). The original Si-O-T band of MK in the region of  $1,300\text{ cm}^{-1}$  no  
 235 longer existed in any of the PM samples due to the dissolution in alkali activator; therefore, the new band  
 236 appeared at  $1,200\text{ cm}^{-1}$  in PM 3/7, representing the Si-OH stretching vibrations in the resulting geopolymers  
 237 (Mo et al., 2014). Furthermore, this band (dash line) progressively shifted to a lower frequency with the  
 238 incremental content of MT, showing that more polycondensation occurred. Another evidence is the bending  
 239 band of Si-O shifting to a lower frequencies ( $700\text{ cm}^{-1}$ ), which was also characterised as the formation of  
 240 geopolymers (Palomo and Glasser, 1992). Two distinct broad bands were situated at approximately  $3,450\text{ cm}^{-1}$   
 241 and  $1,650\text{ cm}^{-1}$ , representing the O-H stretching band and O-H bending band, respectively, which  
 242 indicates the occurrence of polycondensation (Chindapasirt et al., 2009). It is interesting that the sharpest O-  
 243 H stretching ( $3,711\text{ cm}^{-1}$ ) for the trioctahedral group ( $\text{Mg}_3(\text{OH})$ ) practically disappeared, compared to that of  
 244 raw tailings (see Table A.1). This observation can be interpreted to mean that the crystal phlogopite  
 245 degradation likely occurred during the alkali activation. The presence of the band at approximately  $1,460\text{ cm}^{-1}$   
 246  $^{-1}$  in all PM samples has been ascribed to sodium carbonate (Gadsden, 1975). Another significant band  
 247 between  $2,000\text{ to }2,200\text{ cm}^{-1}$  was assigned to the stretching vibration of the functional group of  $\text{Na}_2\text{CO}_3$ ; that  
 248 is, carbonate minerals, generated by reacting alkali activator with MT (Bouaissi, 2019). The hint of the  
 249 formation of cancrinite can be found by the following assignments:  $879\text{ cm}^{-1}$  for C-O bend ( $\text{CO}_3^{2-}$ ) and  $1,400\text{ cm}^{-1}$   
 250  $^{-1}$  for C-O stretch ( $\text{CO}_3^{2-}$ ), which is in line with the results of previous studies (Król et al., 2018; Mozgawa,  
 251 2001; N. Ye et al., 2014). Once combined with the results of XRD, the study indicated that there was no  
 252 crystalline cancrinite in PM 6/4, and the new carbonate mineral was assigned to sodium calcium carbonate  
 253 (Figure 2). Furthermore, the weak bands at  $736\text{ cm}^{-1}$  and  $759\text{ cm}^{-1}$  could be attributed to the formation of T-O  
 254 bonds in the interconnected tetrahedra in PM 6/4. The formation of single four ring (S4R) was in accordance  
 255 with the previous study which stated that the band range of  $720\text{-}760\text{ cm}^{-1}$  is assigned to the formation of  
 256 natrolite zeolite (four-membered rings) (Fernández-Jiménez and Palomo, 2005; Mozgawa, 2001). The new  
 257 peak appeared at  $760\text{ cm}^{-1}$  in the spectrum of PM 7/3 which is assigned to  $\nu_4$  Si-O which was found in other  
 258 blended gel system of C-S-H and N-A-S-H (García-Lodeiro et al., 2008).



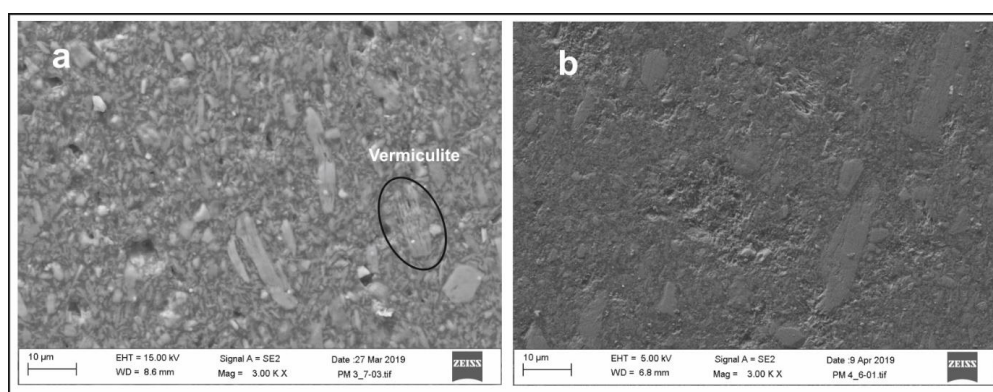
259  
 260 *Figure 3. DRIFT spectra of the tailings-metakaolin based geopolymer samples*

261 **3.3 SEM and EDS**

262 The transformation from phlogopite into vermiculite was observed in PM 3/7 and PM 4/6 (Figure 4), in  
 263 which the morphology resembled the light weight aggregates (expanded vermiculite) implanted in cement



264 matrix (Mladenović et al., 2004). The formation of vermiculite partially resulted from the expended  
265 interlayer of phlogopite by mechanochemical activation; however, it differed from the vermiculite with  $Mg^{2+}$   
266 and  $H_2O$  filling in interlayers (Smith Aitken, 1965). Since the mechanochemically activated MT can release  
267 more  $K^+$  ions during the alkaline activation, it can be replaced by smaller  $Na^+$  ions by cation exchange  
268 forming  $Na^+ \cdot H_2O$  interlayers. From the morphology of PM 3/7, original particles are entrained in the matrix  
269 suggesting a lack of dissolution in PM 3/7. While dissolved particles from MT generate more binder gels in  
270 PM 4/6 (fewer original particles compared to PM 3/7), it can be postulated that the polycondensation stopped  
271 after MK dissolution. The Si/Al ratio for PM 3/7 and PM 4/6 was 1.62 and 1.77, respectively. According to  
272 the research by Oelkers et al. (Oelkers and Gislason, 2001), easily dissolved aluminate units can be adsorbed  
273 on reactant surfaces, thereby decreasing the dissolution of silicate units. This unbalanced dissolution leads to  
274 a lack of formation of geopolymeric linkages. Accompanied with large residues of unreacted MT, the  
275 resulting materials exhibits rather poor mechanical strength.



276  
277 *Figure 4. SEM images of a) PM 3/7 and b) PM 4/6*

278 The gel morphology of PM 5/5 exhibited distinctly different features compared with PM 3/7 and PM 4/6,  
279 where the calcium-rich gel, sodium-deficient matrix (light grey), displayed a clear boundary with the  
280 sodium-rich (darker grey) one according to the elemental mappings (Figure 5). The calcium-rich gel had  
281 unreacted calcite (or crystalline calcite) particles embedded, in which amorphous calcite was the source of  
282 calcium for the generation of C-A-S-H binder. When alkali activators were introduced, amorphous calcite  
283 can react with sodium hydroxide, generating calcium species  $Ca(OH)_2$  (neutral) and  $Na_2Ca(CO_3)_2 \cdot 5H_2O$   
284 (gaylussite). The presence of gaylussite was confirmed by using XRD and DRIFT analyses (Figure 2 and  
285 Figure 3). The monomeric units of Si and Al tetrahedra were dissolved from MK into alkaline activator,  
286 forming N-A-S-H and C-(N)-A-S-H gels. Ca-rich species are prone to react with Ca-bearing species;  
287 thereafter, reaction with Si and Al species occurs. Thus, this phenomenon explains how amorphous calcite  
288 dissolution favours the generation of C-(N)-A-S-H binder, whilst Na-rich regions displayed pronounced  
289 propensity towards N-A-S-H gel. Additionally, at which alkaline concentration is higher than 10 M, the N-  
290 A-S-H gel becomes the main product, whilst C-S-H gel is the secondary phase when calcium hydroxide  
291 exists (Santiago Alonso and Palomo, 2001). Consequently, amorphous carbonate minerals (calcite, dolomite)  
292 can react with the alkaline activator to generate more dissolved calcium ions; these calcium ions are  
293 incorporated in amorphous alkaline aluminosilicate hydrates. The dissolution of calcium ions led to the  
294 formation of a halo in the Ca mapping around the crystalline calcite particles. It can be interpreted that the  
295 boundary between the two gels formed a gaylussite ring (bright green in the Ca map), which resulted from  
296 the high aqueous pH in N-A-S-H gel impeding the dissolution of Ca cation. This gaylussite ring prevented  
297 the interaction between C-(N)-A-S-H and N-A-S-H gels, decreasing the compatibility of these gels which in  
298 turn led to undesirable mechanical properties.

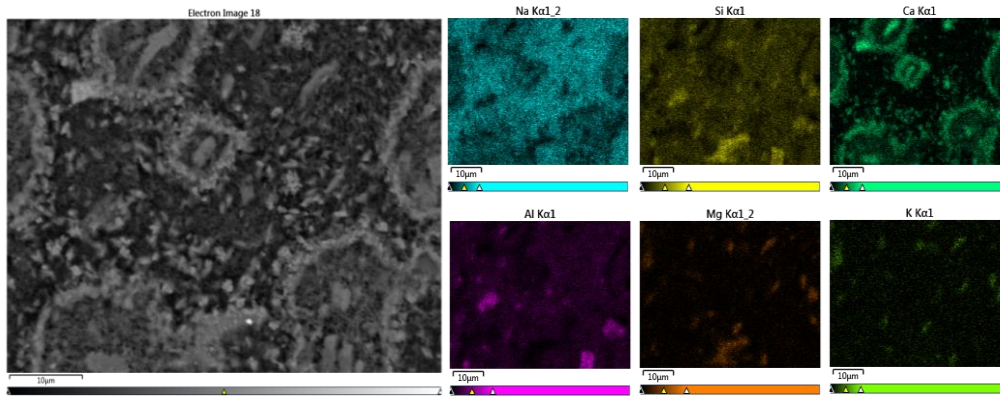
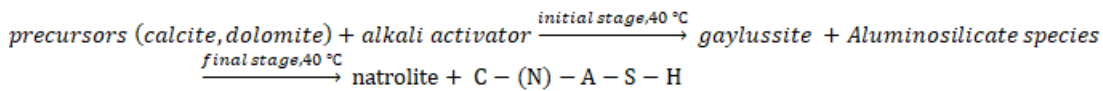


Figure 5. FESEM back-scattered electron (BSE) images and elemental maps for the PM 5/5

299

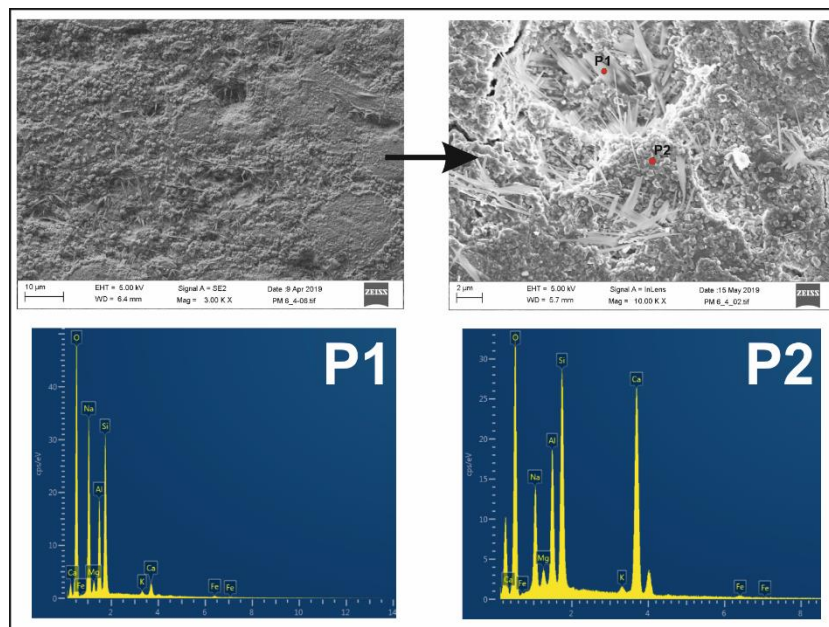
300

301 The scanning electron microscopy (SEM) image of PM 6/4 (Figure 6) reveals the crystallisation of the  
 302 zeolite phase among gel binders. The main substances, natrolite and C-(N)-A-S-H phases, formed in the final  
 303 product after alkali activation. The bundles of fibres or fan-like crystals in PM 6/4 have been ascribed to the  
 304 formation of natrolite zeolite, which was produced by breaking the T-O bonds of chemically reactive  
 305 precursors and regeopolymerisation (Huang et al., 2016; Slaty et al., 2015). The energy dispersive spectra of  
 306 these two phases are provided in Figure 6 (P1 and P2). The nucleation of natrolite has been hypothesised as  
 307 arising from the presence of NaOH, MK, activated MT and the curing conditions as depicted below (El  
 308 Hafid and Hajjaji, 2015).



309

310 There is some evidence to suggest that natrolite is likely formed on the vermiculite where the reflections of  
 311 vermiculite vanished in XRD pattern (Figure 2). Therefore, it is reasonable to assume that the natrolite  
 312 crystallised from the aluminosilicate tetrahedral layers with the supplementation of MK and alkali activator.

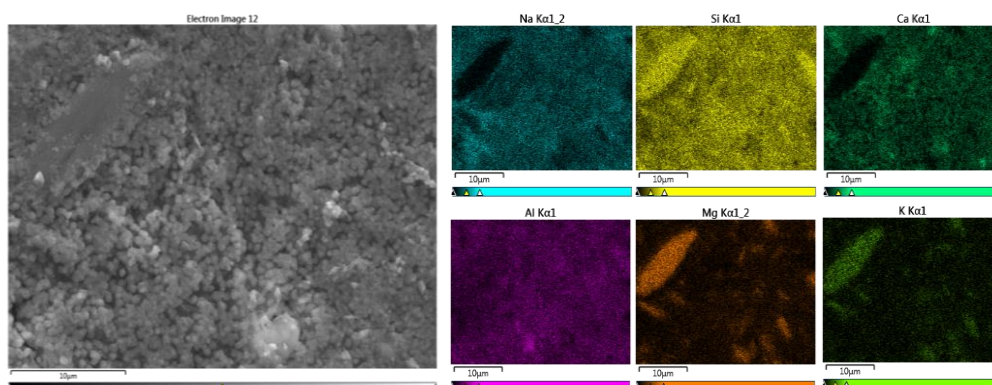


313

314 Figure 6. SEM micrographs of PM 6/4 and energy dispersive spectra of fibrous phase (P1) and gel matrix (P2)

315 In the image of PM 7/3, the tailings-metakaolin based geopolymers consisted of densely geopolymeric  
 316 matrix (Figure 7). The Mg- and K-bearing particles in mapping images represented unreacted MT  
 317 (phlogopite) due to its poor alkali reactivity and structural stability. This result is also in line with its lowest

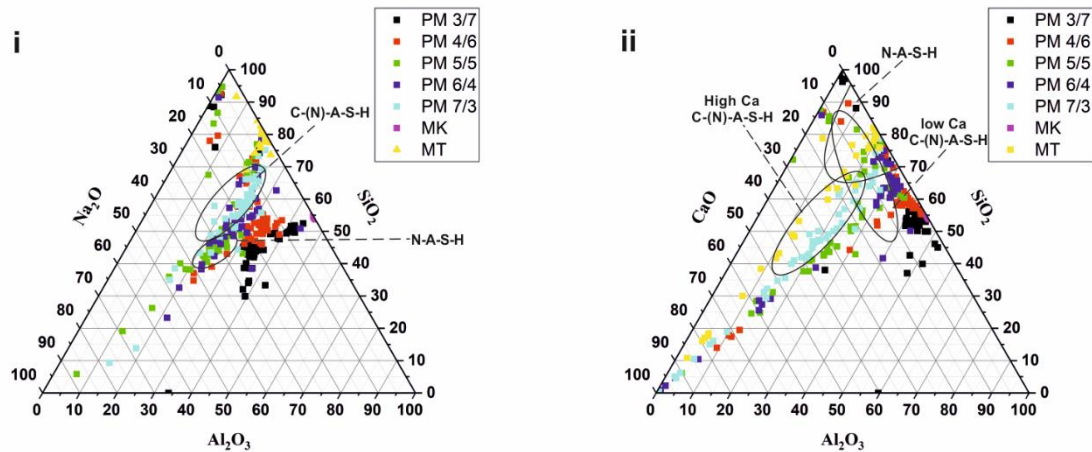
318 apparent porosity. It should be noted that the formation of zeolite-like products results from the alkalinity  
 319 and composition of raw materials (Criado et al., 2007). Unlike chemically reactive raw materials (calcinated  
 320 materials), the inert MT precursor must be first pre-treated in order to supply more soluble aluminosilicate  
 321 phases. In this work, the pre-treatment was still insufficient for the alkali activation, unless the supplement of  
 322 MK for the inadequate aluminium content in phosphate MT. The morphology in the SEM image contained  
 323 column-shaped grains, which has been assigned to the formation of C-(N)-A-S-H phase (S. Chen et al.,  
 324 2010). The generation of C-(N)-A-S-H gel is believed to occur at the expense of N-A-S-H phase through the  
 325 ion exchange mechanism; in addition, PM 7/3 possessed the highest calcium content. This phenomenon was  
 326 ascribed to the assumption proposed by I. Garcia-Lodeiro (Garcia-Lodeiro et al., 2011). Nevertheless, it  
 327 slightly differed from this case regarding to the effect of pH, as the pH was 12.67 (>12) for PM 7/3. The  
 328 existence of C-(N)-A-S-H was confirmed, which meant that the formation of such gel is depended on not  
 329 only the ion exchange mechanism but also the alkaline reaction between carbonate minerals (tailings) and  
 330 MK. Furthermore, it can be hypothesised that the formation of cancrinite is ascribed to the recrystallization  
 331 from C-(N)-A-S-H gel; however, crystalline cancrinite was not observed in the SEM images probably due to  
 332 its scale and the complex matrix of C-(N)-A-S-H gel. From the perspective of UCS, PM 7/3 presents a  
 333 promising UCS compared to other PM samples. Poor mechanical properties have been attributed to the  
 334 amount of crystalline phase in the resulting samples, in which gel-to-crystal transformation leads to the  
 335 reduction of mechanical strength due to the occurrence of open porosity and microcracking occurring in this  
 336 course (Palomo and Glasser, 1992).



337  
 338 *Figure 7. FESEM secondary electron images and elemental maps for the PM 7/3*

339 The mineralogy of MT generates complex compositions in the AAM as displayed in the ternary diagrams  
 340 (Figure 8). The raw tailings barely contained sodium content, whereas it was rich in calcium. Additionally,  
 341 the MT had a wider cluster in the CaO-Al<sub>2</sub>O<sub>3</sub>-SiO<sub>2</sub> diagram, which is due to calcium-containing minerals  
 342 such as calcite and dolomite. Thus, the data of raw tailings are not taken into account during chemical  
 343 analysis in this section. The Na<sub>2</sub>O-Al<sub>2</sub>O<sub>3</sub>-SiO<sub>2</sub> diagram displayed more clustered EDS data points than those  
 344 in the CaO-Al<sub>2</sub>O<sub>3</sub>-SiO<sub>2</sub> counterpart. PM 3/7 exhibited no correlation with geopolymeric gel formation in both  
 345 diagrams, thereby showing rather weak UCS. However, PM 4/6 and PM 5/5 generated N-A-S-H and Na-rich  
 346 C-(N)-A-S-H gel after alkali activation, illustrating the increase of UCS which almost doubled that of PM  
 347 3/7. N-A-S-H gel predominantly formed in the Na<sub>2</sub>O-Al<sub>2</sub>O<sub>3</sub>-SiO<sub>2</sub> system of PM 5/5; these results were  
 348 consistent with the observation in SEM. The data points of PM 6/4 located in the N-A-S-H gel area which  
 349 are genuinely assigned to the natrolite, and the Na-rich C-(N)-A-S-H gel which has confirmed in preceding  
 350 results. With MT content increased to 70%, it promotes the formation of C-(N)-A-S-H gel and the  
 351 (re)crystallisation of cancrinite is developed. Compared with PM 7/3, PM 5/5 and PM 6/4 predominantly  
 352 consisted of Na-rich C-(N)-A-S-H gel.





353

354 *Figure 8. Projection of alkali-activated materials chemistry onto the i) Na<sub>2</sub>O-Al<sub>2</sub>O<sub>3</sub>-SiO<sub>2</sub> ternary diagram and ii) CaO-*  
 355 *Al<sub>2</sub>O<sub>3</sub>-SiO<sub>2</sub> ternary diagram showing the elemental composition of cured PM samples for 7 days and raw materials. The*  
 356 *regions of C-(N)-A-S-H and N-A-S-H were approximately from (Walkley et al., 2016), (Ismail et al., 2014) and (van*  
 357 *Deventer et al., 2015).*

358 The ternary diagram explicitly illustrated the development of gel formation with the increasing tailings  
 359 content. At a lower content of sodium ions (Na/Al<1), the accumulation of free alumina units occurred,  
 360 thereby preventing further polycondensation. With the incremental Na/Al ratio, it facilitated the alkali  
 361 activation; thereafter, it produced not only N-A-S-H gel but also C-(N)-A-S-H gel after the appearance of  
 362 sodium calcium carbonate and calcium hydroxide.

### 363 3.4 <sup>29</sup>Si and <sup>27</sup>Al MAS NMR

364 The results of the NMR analysis are shown in Figure 9. Among all the products, analysis was performed for  
 365 three samples: PM 3/7, PM 5/5 and PM 7/3 (which have low, medium and high compressive strength,  
 366 respectively). Among all the reactants, measurements were done only for MK. Measurement of MT was  
 367 unsuccessful due to its high iron content.

368 The results of the <sup>29</sup>Si NMR analysis are depicted in Figure 9a. The spectrum of MK displayed a broad  
 369 amorphous component involving mainly Q<sup>4</sup> and Q<sup>3</sup> species. The high strength product, PM 7/3, displayed  
 370 mainly Q<sup>2</sup> species, which indicated the presence of non-cross-linked C-(N)-A-S-H units. The spectrum of  
 371 medium strength product PM 5/5 was similar to PM 7/3, except there was a slight shift of the main peak to  
 372 the right (indicating more non-cross-linked C-(N)-A-S-H phase) and the emergence of a small hump  
 373 converting Q<sup>4</sup> and Q<sup>3</sup> species (indicating N-A-S-H phase). In the case of the low-strength sample, PM 3/7,  
 374 the most dominant feature was a strong peak close to Q<sup>4</sup> and Q<sup>3</sup> species (indicating N-A-S-H phase). It is  
 375 also possible that Q<sup>3</sup> species formed part of cross-linked C-(N)-A-S-H. Contribution from Q<sup>2</sup> species was a  
 376 shoulder feature (indicating presence of non-cross-linked C-(N)-A-S-H). Another important feature of this  
 377 sample is a considerable broad hump covering Q<sup>1</sup> and Q<sup>0</sup> species. This feature indicated the presence of  
 378 sodium silicate species, which do not contribute to compressive strength like C-(N)-A-S-H. This is one of the  
 379 reasons for PM3/7 displaying low strength.

380 The results of the <sup>27</sup>Al NMR analysis of are depicted in Figure 9b. MK consists of tetrahedral, pentahedral  
 381 and octahedral aluminum species. The high-strength product, PM 7/3 consisted tetrahedral aluminum  
 382 species, which indicated the presence of non-cross-linked C-(N)-A-S-H units. The spectrum of medium  
 383 strength product PM 5/5 was similar to PM 7/3, except for the slight shift of the tetrahedral peak to the left.  
 384 In the case of the low strength sample (PM 3/7), a similar tetrahedral component was visible. Notably, C-  
 385 (N)-A-S-H had tetrahedral aluminum; hence, the spectra of all the products exhibited a similar tetrahedral  
 386 component. However, there was a small shift of this component towards right as we move from PM 7/3 to  
 387 PM 3/7. This feature was due to the fact that the chemical shift values of aluminum follows the order: (Al<sup>4</sup>  
 388 in q<sup>2</sup>) > (Al<sup>4</sup> in q<sup>3</sup>) > (Al<sup>4</sup> in q<sup>4</sup>) (Houston et al., 2009; Myers et al., 2015). The low strength sample PM 3/7

389 displayed an additional component at approximately 80 ppm which may belong to low-connectivity  
 390 aluminate species (Faust and Ribeiro, n.d.; Sagoe-Crentsil and Weng, 2006). Since these species do not  
 391 contribute to strength-enhancing C-(N)-A-S-H phase, it may contribute towards the low strength of PM 3/7.

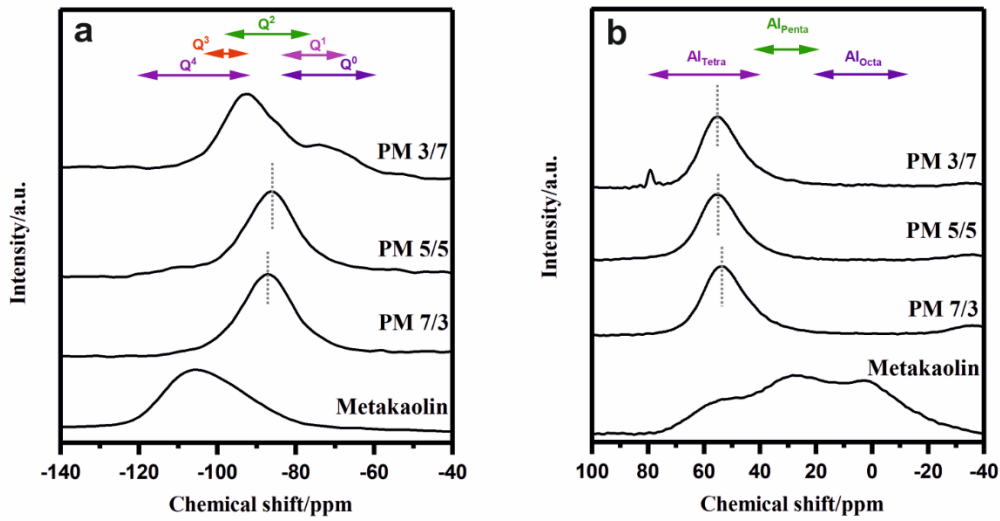
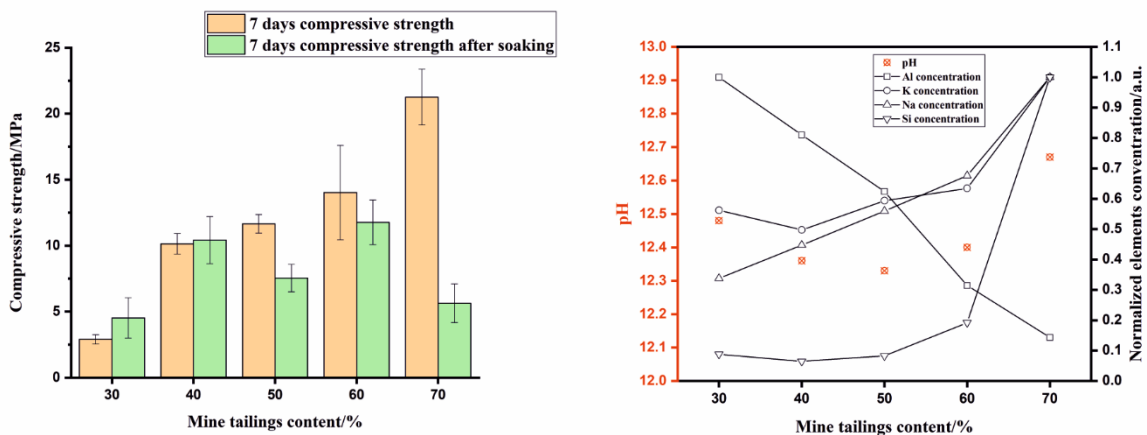


Figure 9. The results of a)  $^{29}\text{Si}$  NMR and b)  $^{27}\text{Al}$  NMR analysis for products and reactants.

### 394 3.5 Soaking test

395 The soaking test can affect the UCS of PM samples (Figure 10), and the decrease of UCS has also been  
 396 observed in other studies (Boutterin and Davidovits, 2003). There is a synergetic effect between the swelling  
 397 pressure and regeopolymerization for PM samples. For PM 3/7 and PM 4/6, there is a significant leaching of  
 398 Al species which means that the geopolymeric reaction was unfulfilled, furthermore, there was less  
 399 formation of aluminosilicate hydrates indicating a weak and porous matrix. However, dissolvable Al species  
 400 took part in the regeopolymerization, which expresses large effect than swelling repulsion between particles  
 401 resulting in a higher soaked strength. There is a different situation for PM 5/5, PM 6/4 and PM 7/3, where  
 402 geopolymerization was achieved thereby the effect of swelling pressure is more conspicuous, leading to a  
 403 lower strength.

404 The filtrate was collected and subjected to ICP-OES analysis. The least leaching of sodium concentration in  
 405 PM 3/7 could be attributed to the strongly bonded sodium cations with negative units such as  $\text{Si}_4\text{O}_8(\text{OH})_6^{4-}$ ,  
 406  $\text{SiO}(\text{OH})_3^-$  and  $\text{SiO}_2(\text{OH})_2^{2-}$ , forming a rather weak matrix (Panias et al., 2007). Another piece of evidence is  
 407 the high concentration of Al in solution, indicating a lower amount of aluminium taken part in alkali  
 408 activation.

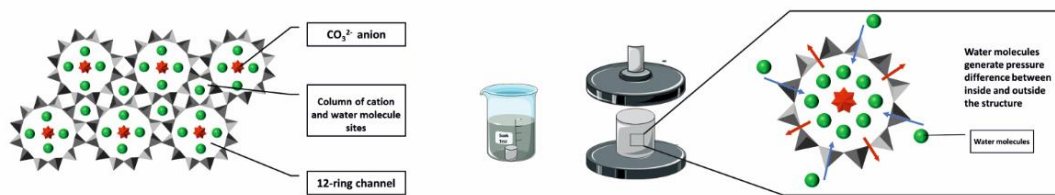




410 *Figure 10. a) compressive strength of tailings-metakaolin geopolymer samples after soaking in DI water for 24 h, b)*  
411 *ICP-OES analysis and pH of the liquid after soaking test*

412 As for PM 5/5 and PM 6/4, they consisted of lower amounts of C-(N)-A-S-H gel, revealing the decrease of  
413 UCS. It is reasonable to assume that C-(N)-A-S-H gel has higher water-solubility, when compared with N-A-  
414 S-H and C-A-S-H gels. Another assumption is that  $K^+$  ions were dissolved from more soluble phases, and  
415 this induced capillary force resulting in microcracks within interfaces or grain boundaries.

416 PM 7/3 had the highest degree of alkali activation and displayed the lowest leaching content of aluminium  
417 among all PM samples. Interestingly, it was the sample that was most affected by the 24-h soaking,  
418 simultaneously showing the lowest water absorption and porosity (Figure 1b). These findings might be  
419 explained by the presence of cancrinite (Figure 11). Structural alternation occurred in the cancrinite-like (C-  
420 N-A-S-H) gel, in which water can easily penetrate into the cancrinite structure. Cancrinite can be found in  
421 nature as a porous mineral, of which the fundamental layers of six-membered rings of  $SiO_4$  and  $AlO_4$   
422 tetrahedra are stacked along the c-axis in an AB-AB sequence (Hackbarth et al., 1999). There are two types  
423 of cages within cancrinite structures: 11-hedral cavities and  $\epsilon$ -cages along with 12-ring channels as depicted  
424 in Figure 11. The largest discrepancy of UCS in PM 7/3 after soaking might be explained by the structural  
425 destabilisation of cancrinite-like (C-N-A-S-H) gel, in which water can easily stab into cancrinite structure.  
426 Moreover, the limited space in cages and clogged channels results in the blocking of pore structure, thereby  
427 preventing extra water entering. It continues exerting pressure to the porous structure during cage expansion,  
428 leading to the low UCS (Liu et al., 2007). Therefore, the weakened alkali-activated structures presented  
429 undesirable compressive strength after a 24-h soaking, displaying the lowest water absorption and porosity.



430  
431 *Figure 11. Schematic structure change of cancrinite after soaking test (aluminosilicate tetrahedra in grey).*

### 432 433 3.6. Life cycle assessment

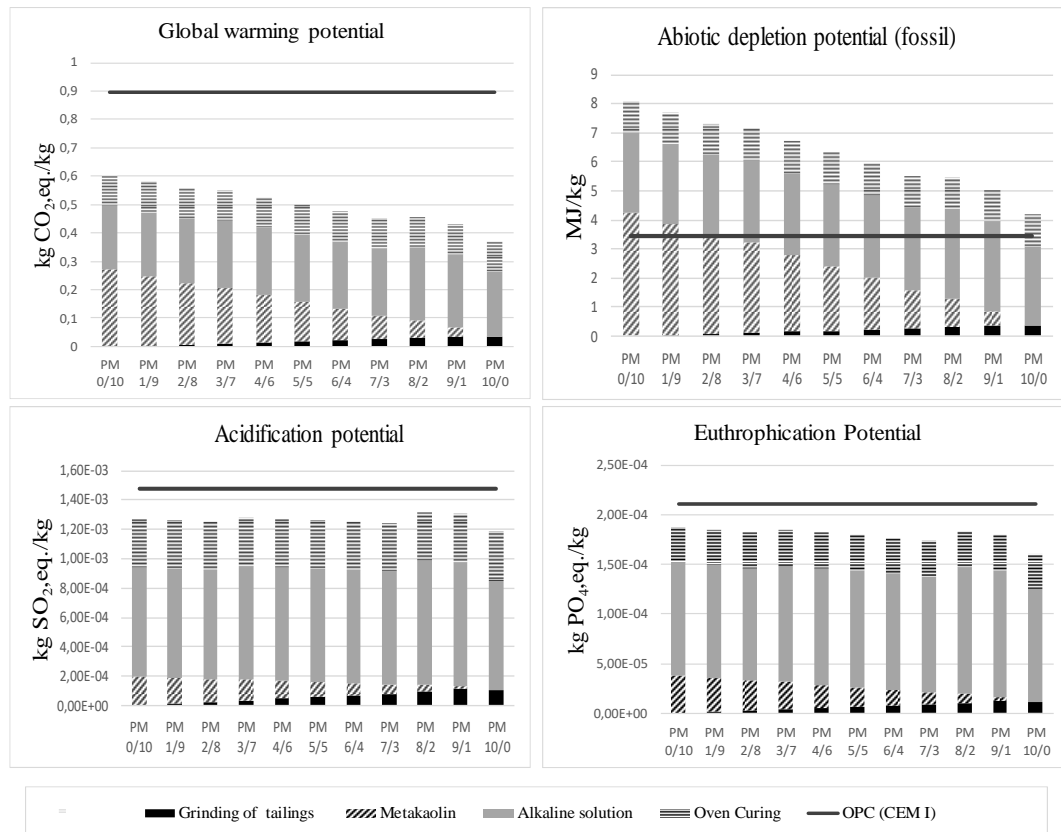
434 Figure 12 shows GWP, AP, EP and ADP (fossil) LCA results for the different alkali-activated binders in  
435 comparison to OPC. For the strongest alkali-activated binder PM 7/3, excellent performances were exhibited  
436 in impact categories GWP, AP and EP, with 50%, 16% and 18% less emissions than Portland cement,  
437 respectively. The significant contributors in these impact categories for PM 7/3 were the alkaline solution  
438 (sodium silicate and sodium hydroxide) and curing which accounted for 52% and 24% respectively for  
439 GWP, 62% and 27% respectively for AP, and 67% and 21% for EP.

440 Furthermore, regarding PM 7/3, ADP (fossil) displayed a significant 61% increase in energy consumption  
441 when compared to Portland cement, with alkaline solution, MK and curing; contributing 51%, 24% and 20%  
442 respectively. The high amount of energy is associated with energy consumed during production of alkaline  
443 solution (Fawer et al., 1999) and in calcining kaolin to MK (Heath et al., 2014). Phosphate mining  
444 beneficiation exhibited minimal contribution (less than 10%) in all impact categories. This is because only  
445 beneficiation impacts were considered, as phosphate tailings were considered as wastes in this study.  
446 Furthermore, MK displayed minimal contribution in AP and EP impact categories, but slightly higher  
447 contribution in GWP (19%).

448 Phosphate MT and MK alkali-activated binders have shown a significant reduction in global warming; in  
449 particular they constitute only 8% of global  $CO_2$  emissions (Andrew, 2018). Alkaline solution has been

450 highlighted as the material that contribute the most to the environmental burdens of alkali-activated binders,  
 451 and studies have recommended using silica rich waste materials as a substitute to conventional alkaline  
 452 solution (Abdulkareem et al., 2019; Passuello et al., 2017). With respect to curing, waste heat can be used for  
 453 energy, thereby increasing the environmental performance of the binder.

454 This LCA study highlights the relevance of using waste materials in the development of alkali-activated  
 455 binders. Not only are significant impact reductions achieved, but a useful alternative to simply disposing  
 456 waste residues (which may eventually lead to contamination) is provided.



457

458

Figure 12. Life cycle impact assessment results for alkali-activated binder in comparison to CEM I.

## 459 5. Conclusion

460 This study investigated the synthesis of AAM using mechanochemically activated phosphate MT with MK  
 461 as (calcium) aluminosilicate precursors. The geopolymer with the higher content of tailings (60% to 70%)  
 462 displayed the best mechanical properties (>20 MPa).

463 There were two main factors to consider: 1) The mechanochemical activation improves the chemical  
 464 reactivity of tailings, and 2) the presence of calcium-rich carbonate minerals accelerates the formation of C-  
 465 (N)-A-S-H binder. The chemical process of alkali-activated phosphate tailings-metakaolin based  
 466 geopolymers appear to more complicated due to the appearance of the C-(N)-A-S-H binder. New zeolites,  
 467 such as natrolite (which was fibre-like) and cancrinite (which was column-like) formed.

468 With the increment of tailings quantity (>70%), water requirement was lowered due to more favourable  
 469 particle shape. Although the highest compressive strength was achieved with 70% tailings, water resistance  
 470 in PM 7/3 still required further improvement. The recycling of MT significantly depends on its chemical and  
 471 mineralogical composition, and its interactions with alkaline activators.

472 From the view of circular economy, this study provides a potential method to recycle mine tailings with high  
 473 added value rather than landfill or impoundment. The manufacturing of tailings-based geopolymers gives  
 474 huge opportunities for local availability such as minimizing traffic expense and maximizing sustainability.

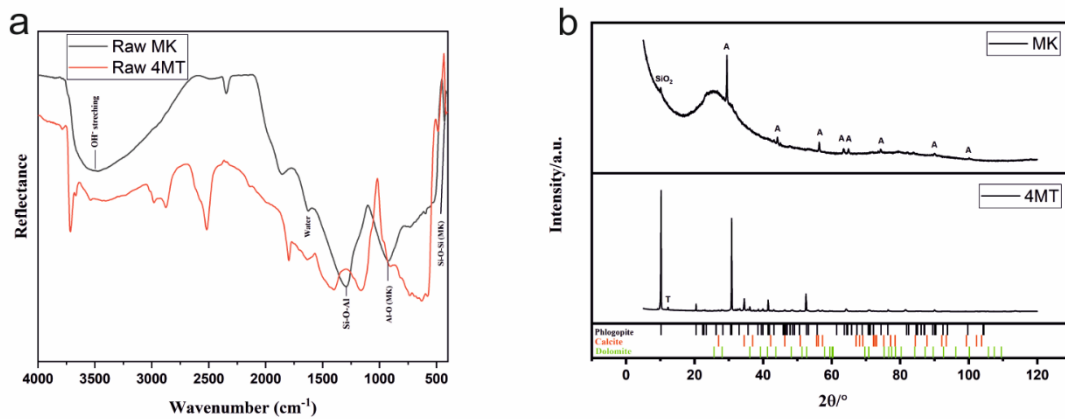
475 Particularly, it considerably decreases CO<sub>2</sub> emissions in comparison with OPC. According to the  
 476 performance of tailings-based geopolymers, such a material displayed promising properties for construction  
 477 applications, such as brick manufacturing.

478 **Acknowledgement**

479 The authors gratefully acknowledge the financial support from the Academy of Finland [grants #292526,  
 480 #319676 and #326291] and the European Union’s EU Framework Programme for Research and Innovation  
 481 Horizon 2020 [Grant Agreement No 812580 (“SULTAN”, <https://etn-sultan.eu>)]. The authors would like to  
 482 thank Pasi Juntunen for the assistance in FESEM measurement, Mr. Pekka Tanskanen and Mr. Marcin Selent  
 483 for their assistance in XRD analysis, Mr. Aki-Petteri Pokka for the assistance in compressive strength  
 484 measurement. Mr. Jarno Karvonen and Mr. Jani Österlund are acknowledged for their contribution in  
 485 laboratory experiments. V.-V.T. thanks the Academy of Finland (grants #289649, 294027 and 319216) for  
 486 the financial support.

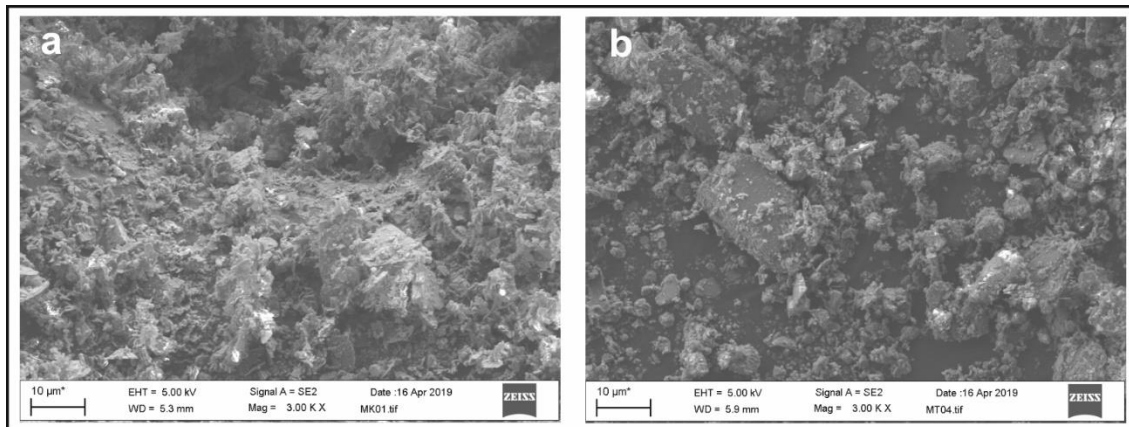
487 **Appendix A. Fundamental information of precursors**

488



489

490 *Figure A.1. a) DRIFT spectra of raw materials b) XRD patterns of raw materials. SiO<sub>2</sub> (#04-007-2627), A: anatase*  
 491 *(#00-064-0803), T: tremolite (#04-013-2249).*



492

493 *Figure A.2. a) SEM secondary electron micrographs of metakaolin, b) SEM secondary electron micrographs of 4-min*  
 494 *ground phosphate mine tailings.*

495

*Table A.1. Description of main bands of 4-min ground phosphate mine tailings*

Wavenumber (cm <sup>-1</sup> )	Band characterization	Reference
3711	OH-stretching vibration (phlogopite)	(Bigham et al.,

		2001; Farmer, 1974; Schingaro et al., 2013)
3665	OH-stretching vibration Group I (tremolite)	(Najorka and Gottschalk, 2003)
3535	OH-stretching vibration Group III (tremolite)	(Najorka and Gottschalk, 2003)
2979	Carbonate $\nu_2$ overtone (dolomite)	(Messerschmidt, 1985; Nguyen et al., 1991)
2873	Carbonate (calcite)	(Messerschmidt, 1985; Nguyen et al., 1991)
2519	$2\nu_2+\nu_4$ combination mode (dolomite, calcite)	(Gunasekaran and Anbalagan, n.d.; Nguyen et al., 1991)
1795	Carbonate (calcite)	(Nguyen et al., 1991)
1635	Carbonate $\nu_3$ (apatite)	(Bigham et al., 2001; Rehman and Bonfield, 1997)
1395	C-O Asymmetric stretching $\nu_3$ (dolomite, calcite)	(Clark, n.d.)
1162	Si-O-T (T: Si or Al) (phlogopite)	(Rees et al., 2007)
974	Non-diagnostic Si-O stretching (phlogopite)	(Bigham et al., 2001; Farmer, 1974)
905	Out-of-plane bending $\nu_2$ (dolomite, calcite)	(Farmer, 1974; Rehman and Bonfield, 1997)
823	Apical Al-O bond from $\text{AlO}_4$ (phlogopite)	(Bigham et al., 2001; Farmer, 1974)
732	In-plane bending $\nu_4$ (dolomite, calcite)	(Gunasekaran and Anbalagan, n.d.)
693	Perpendicular vibration (phlogopite)	(Bigham et al., 2001; Farmer, 1974)
665	In-plane vibration of Al-O-Si (phlogopite)	(Bigham et al., 2001; Farmer, 1974)
628	OH vibration (phlogopite)	(Bigham et al., 2001; Farmer, 1974)
579	Asymmetric deformation $\nu_4$ (apatite)	(Veiderma et al., 1998)

496

497 [Appendix B. Data sources for Life cycle inventory](#)

498

499

*Table B.1. Data sources*

Type of data	Source
--------------	--------

Sodium hydroxide	GaBi database 2019 (EU-28, sodium hydroxide, 100% caustic soda)
Sodium silicate solution	(Fawer et al., 1999) (sodium silicate 3.3, furnace liquor, 37% solid)
Cement	(CEMBUREAU, 2015) (OPC CEM I)
Metakaolin	Heath et al., 2014; NLK, 2002
Water	GaBi database, 2019 (EU- 28, tap water)
Electricity	GaBi database, 2019 (Finland, electricity grid mix)

500

## 501 References

- 502 Abdulkareem, M., Havukainen, J., Horttanainen, M., 2019. How environmentally sustainable are  
503 fibre reinforced alkali-activated concretes? *J. Clean. Prod.* 236.  
504 <https://doi.org/10.1016/J.JCLEPRO.2019.07.076>
- 505 Ahmari, S., Zhang, L., 2013. Utilization of cement kiln dust (CKD) to enhance mine tailings-based  
506 geopolymer bricks. *Constr. Build. Mater.* 40, 1002–1011.  
507 <https://doi.org/10.1016/j.conbuildmat.2012.11.069>
- 508 Alonso, Santiago, Palomo, A., 2001. Calorimetric study of alkaline activation of calcium  
509 hydroxide–metakaolin solid mixtures. *Cem. Concr. Res.* 31, 25–30.  
510 [https://doi.org/10.1016/S0008-8846\(00\)00435-X](https://doi.org/10.1016/S0008-8846(00)00435-X)
- 511 Alonso, S, Palomo, A., 2001. Alkaline activation of metakaolin and calcium hydroxide mixtures:  
512 influence of temperature, activator concentration and solids ratio. *Mater. Lett.* 47, 55–62.  
513 [https://doi.org/10.1016/S0167-577X\(00\)00212-3](https://doi.org/10.1016/S0167-577X(00)00212-3)
- 514 R.M. Andrew, Global CO<sub>2</sub> emissions from cement production, *Earth Syst Sci Data.* 105194 (2018)  
515 195–21710.
- 516 Bakharev, T., 2005. Resistance of geopolymer materials to acid attack. *Cem. Concr. Res.* 35, 658–  
517 670.
- 518 Balczár, I., Korim, T., Kovács, A., Makó, É., 2016. Mechanochemical and thermal activation of  
519 kaolin for manufacturing geopolymer mortars–Comparative study. *Ceram. Int.* 42, 15367–  
520 15375.
- 521 Bigham, J.M., Bhatti, T.M., Vuorinen, A., Tuovinen, O.H., 2001. Dissolution and structural  
522 alteration of phlogopite mediated by proton attack and bacterial oxidation of ferrous iron.  
523 *Hydrometallurgy* 59, 301–309. [https://doi.org/10.1016/S0304-386X\(00\)00186-9](https://doi.org/10.1016/S0304-386X(00)00186-9)
- 524 Boldyreva, E., 2013. Mechanochemistry of inorganic and organic systems: what is similar, what is  
525 different? *Chem. Soc. Rev.* 42, 7719. <https://doi.org/10.1039/c3cs60052a>
- 526 Bouaissi, A., 2019. Mechanical properties and microstructure analysis of FA-GGBS-HMNS based  
527 geopolymer concrete. *Constr. Build. Mater.* 12.
- 528 Bouterin, C., Davidovits, J., 2003. Réticulation géopolymérique (LTGS) et matériaux de  
529 construction. *Géopolymère* 1, 79–88.
- 530 CEMBUREAU, 2015. Environmental Product Declaration (EPD) Portland Cement (CEM I)  
531 produced in Europe.
- 532 Chen, C., Habert, G., Bouzidi, Y., Jullien, A., 2010. Environmental impact of cement production:  
533 detail of the different processes and cement plant variability evaluation. *J. Clean. Prod.* 18,  
534 478–485. <https://doi.org/10.1016/j.jclepro.2009.12.014>
- 535 Chen, S., Wu, M., Zhang, S., 2010. Mineral phases and properties of alkali-activated metakaolin-  
536 slag hydroceramics for a disposal of simulated highly-alkaline wastes. *J. Nucl. Mater.* 402,  
537 173–178. <https://doi.org/10.1016/j.jnucmat.2010.05.015>
- 538 Chindaprasirt, P., Jaturapitakkul, C., Chalee, W., Rattanasak, U., 2009. Comparative study on the  
539 characteristics of fly ash and bottom ash geopolymers. *Waste Manag.* 29, 539–543.  
540 <https://doi.org/10.1016/j.wasman.2008.06.023>



541 Clark, R.N., n.d. Spectroscopy of Rocks and Minerals, and Principles of Spectroscopy 64.  
542 Criado, M., Fernández-Jiménez, A., de la Torre, A.G., Aranda, M.A.G., Palomo, A., 2007. An XRD  
543 study of the effect of the SiO<sub>2</sub>/Na<sub>2</sub>O ratio on the alkali activation of fly ash. *Cem. Concr.*  
544 *Res.* 37, 671–679. <https://doi.org/10.1016/j.cemconres.2007.01.013>  
545 P. Duxson, J.L. Provis, G.C. Lukey, J.S.J. van Deventer, The role of inorganic polymer technology  
546 in the development of 'green concrete', *Cem. Concr. Res.* 37 (2007) 1590–1597.  
547 [doi:10.1016/j.cemconres.2007.08.018](https://doi.org/10.1016/j.cemconres.2007.08.018).  
548 El Hafid, K., Hajjaji, M., 2015. Effects of the experimental factors on the microstructure and the  
549 properties of cured alkali-activated heated clay. *Appl. Clay Sci.* 116–117, 202–210.  
550 <https://doi.org/10.1016/j.clay.2015.03.015>  
551 EN ISO 14040, 2006. SFS-EN ISO 14040 ENVIRONMENTAL MANAGEMENT. LIFE CYCLE  
552 ASSESSMENT . PRINCIPLES AND FRAME- WORK (ISO 14040 : 2006).  
553 EN, T., 2007. Natural stone test methods-Determination of real density and apparent density, and of  
554 total and open porosity. *Turk. Stand. Inst. Ank.* 13.  
555 Farmer, V.C., 1974. Infrared spectra of minerals. Mineralogical society.  
556 Faust, B.C., Ribeiro, A., n.d. Speciation of aqueous mononuclear Al(III)-hydroxo and other Al (III)  
557 complexes at concentrations of geochemical relevance by aluminum-27 nuclear magnetic  
558 resonance spectroscopy 11.  
559 Fawer, M., Concannon, M., Rieber, W., 1999. Life cycle inventories for the production of sodium  
560 silicates. *Int. J. Life Cycle Assess.* 4, 207–212. <https://doi.org/10.1007/BF02979498>  
561 Fernández-Jiménez, A., Palomo, A., 2005. Mid-infrared spectroscopic studies of alkali-activated fly  
562 ash structure. *Microporous Mesoporous Mater.* 86, 207–214.  
563 <https://doi.org/10.1016/j.micromeso.2005.05.057>  
564 J.A. Gadsden, Infrared spectra of minerals and related inorganic compounds, 1975.  
565 García-Lodeiro, I., Fernández-Jiménez, A., Blanco, M.T., Palomo, A., 2008. FTIR study of the sol-  
566 gel synthesis of cementitious gels: C-S-H and N-A-S-H. *J. Sol-Gel Sci. Technol.* 45, 63-  
567 72. <https://doi.org/10.1007/s10971-007-1643-6>  
568 García-Lodeiro, I., Fernández-Jiménez, A., Palomo, A., Macphee, D.E., 2010. Effect of Calcium  
569 Additions on N-A-S-H Cementitious Gels. *J. Am. Ceram. Soc.*  
570 <https://doi.org/10.1111/j.1551-2916.2010.03668.x>  
571 Garcia-Lodeiro, I., Palomo, A., Fernández-Jiménez, A., Macphee, D.E., 2011. Compatibility studies  
572 between N-A-S-H and C-A-S-H gels. Study in the ternary diagram Na<sub>2</sub>O–CaO–Al<sub>2</sub>O<sub>3</sub>–  
573 SiO<sub>2</sub>–H<sub>2</sub>O. *Cem. Concr. Res.* 41, 923–931. <https://doi.org/10.1016/j.cemconres.2011.05.006>  
574 Gunasekaran, S., Anbalagan, G., n.d. Thermal decomposition of natural dolomite 6.  
575 K. Hackbarth, T.M. Gesing, M. Fechteldord, F. Stief, Synthesis and crystal structure of carbonate  
576 cancrinite Na<sub>8</sub>[AlSiO<sub>4</sub>]<sub>6</sub>CO<sub>3</sub>(H<sub>2</sub>O)<sub>3.4</sub>, grown under low-temperature hydrothermal  
577 conditions, *Microporous Mesoporous Mater.* (1999) 12.  
578 A. Hasanbeigi, C. Menke, L. Price, The CO<sub>2</sub> abatement cost curve for the Thailand cement industry,  
579 *J. Clean. Prod.* 18 (2010) 1509–1518. [doi:10.1016/j.jclepro.2010.06.005](https://doi.org/10.1016/j.jclepro.2010.06.005).  
580 Heath, A., Paine, K., McManus, M., 2014. Minimising the global warming potential of clay based  
581 geopolymers. *J. Clean. Prod.* 78, 75–83. <https://doi.org/10.1016/j.jclepro.2014.04.046>  
582 Houston, J.R., Maxwell, R.S., Carroll, S.A., 2009. Transformation of meta-stable calcium silicate  
583 hydrates to tobermorite: reaction kinetics and molecular structure from XRD and NMR  
584 spectroscopy. *Geochem. Trans.* 10, 1. <https://doi.org/10.1186/1467-4866-10-1>  
585 Huang, X., Huang, T., Li, S., Muhammad, F., Xu, G., Zhao, Z., Yu, L., Yan, Y., Li, D., Jiao, B.,  
586 2016. Immobilization of chromite ore processing residue with alkali-activated blast furnace  
587 slag-based geopolymer. *Ceram. Int.* 42, 9538–9549.  
588 <https://doi.org/10.1016/j.ceramint.2016.03.033>  
589 Ismail, I., Bernal, S.A., Provis, J.L., San Nicolas, R., Hamdan, S., van Deventer, J.S.J., 2014.  
590 Modification of phase evolution in alkali-activated blast furnace slag by the incorporation of

- 591 fly ash. Cem. Concr. Compos. 45, 125–135.  
592 <https://doi.org/10.1016/j.cemconcomp.2013.09.006>
- 593 Kauppila, P., Räsänen, M.L., Myllyoja, S., 2013. Best Environmental Practices in Metal Ore  
594 Mining (Metallimalmikaivostoiminnan parhaat ympäristökäytännöt).
- 595 Kinnunen, P., Ismailov, A., Solismaa, S., Sreenivasan, H., Räsänen, M.-L., Levänen, E., Illikainen,  
596 M., 2018. Recycling mine tailings in chemically bonded ceramics – A review. *J. Clean.*  
597 *Prod.* 174, 634–649. <https://doi.org/10.1016/j.jclepro.2017.10.280>
- 598 M. Król, P. Rožek, W. Mozgawa, Preparation and Structure of Geopolymer-Based Alkali-Activated  
599 Circulating Fluidized Bed Ash Composite for Removing Ni<sup>2+</sup> from Wastewater, in: D.  
600 Singh, M. Fukushima, Y.-W. Kim, K. Shimamura, N. Imanaka, T. Ohji, J. Amoroso, M.  
601 Lanagan (Eds.), *Ceram. Trans. Ser.*, John Wiley & Sons, Inc., Hoboken, NJ, USA, 2018: pp.  
602 147–154. doi:10.1002/9781119494096.ch15.
- 603 Liu, Q., Navrotsky, A., Jove-Colon, C.F., Bonhomme, F., 2007. Energetics of cancrinite: Effect of  
604 salt inclusion. *Microporous Mesoporous Mater.* 98, 227–233.  
605 <https://doi.org/10.1016/j.micromeso.2006.09.008>
- 606 MacKenzie, K.J.D., Brew, D.R.M., Fletcher, R.A., Vagana, R., 2007. Formation of aluminosilicate  
607 geopolymers from 1:1 layer-lattice minerals pre-treated by various methods: a comparative  
608 study. *J. Mater. Sci.* 42, 4667–4674. <https://doi.org/10.1007/s10853-006-0173-x>
- 609 Maragkos, I., Giannopoulou, I.P., Pantias, D., 2009. Synthesis of ferronickel slag-based  
610 geopolymers. *Miner. Eng.* 22, 196–203. <https://doi.org/10.1016/j.mineng.2008.07.003>
- 611 Merrild, H., Larsen, A.W., Christensen, T.H., 2012. Assessing recycling versus incineration of key  
612 materials in municipal waste: The importance of efficient energy recovery and transport  
613 distances. *Waste Manag.* 32, 1009–1018. <https://doi.org/10.1016/J.WASMAN.2011.12.025>
- 614 Messerschmidt, R.G., 1985. Complete Elimination of Specular Reflectance in Infrared Diffuse  
615 Reflectance Measurements. *Appl. Spectrosc.* 39, 737–739.  
616 <https://doi.org/10.1366/0003702854250167>
- 617 Mladenovič, A., Šuput, J.S., Ducman, V., Škapin, A.S., 2004. Alkali–silica reactivity of some  
618 frequently used lightweight aggregates. *Cem. Concr. Res.* 34, 1809–1816.  
619 <https://doi.org/10.1016/j.cemconres.2004.01.017>
- 620 Mo, B., Zhu, H., Cui, X., He, Y., Gong, S., 2014. Effect of curing temperature on  
621 geopolymerization of metakaolin-based geopolymers. *Appl. Clay Sci.* 99, 144–148.  
622 <https://doi.org/10.1016/j.clay.2014.06.024>
- 623 Moukannaa, S., Loutou, M., Benzaazoua, M., Vitola, L., Alami, J., Hakkou, R., 2018. Recycling of  
624 phosphate mine tailings for the production of geopolymers. *J. Clean. Prod.* 185, 891–903.  
625 <https://doi.org/10.1016/j.jclepro.2018.03.094>
- 626 Moukannaa, S., Nazari, A., Bagheri, A., Loutou, M., Sanjayan, J.G., Hakkou, R., 2019. Alkaline  
627 fused phosphate mine tailings for geopolymer mortar synthesis: Thermal stability,  
628 mechanical and microstructural properties. *J. Non-Cryst. Solids* 511, 76–85.  
629 <https://doi.org/10.1016/j.jnoncrysol.2018.12.031>
- 630 Mozgawa, W., 2001. The relation between structure and vibrational spectra of natural zeolites. *J.*  
631 *Mol. Struct.* 596, 129–137. [https://doi.org/10.1016/S0022-2860\(01\)00741-4](https://doi.org/10.1016/S0022-2860(01)00741-4)
- 632 Mucsi, G., Kumar, S., Csöke, B., Kumar, R., Molnár, Z., Rácz, Á., Mádai, F., Debreczeni, Á., 2015.  
633 Control of geopolymer properties by grinding of land filled fly ash. *Int. J. Miner. Process.*  
634 143, 50–58. <https://doi.org/10.1016/j.minpro.2015.08.010>
- 635 Myers, R.J., Bernal, S.A., Gehman, J.D., van Deventer, J.S.J., Provis, J.L., 2015. The Role of Al in  
636 Cross-Linking of Alkali-Activated Slag Cements. *J. Am. Ceram. Soc.* 98, 996–1004.  
637 <https://doi.org/10.1111/jace.13360>
- 638 Najorka, J., Gottschalk, M., 2003. Crystal chemistry of tremolite-tschermakite solid solutions. *Phys.*  
639 *Chem. Miner.* 30, 108–124. <https://doi.org/10.1007/s00269-002-0291-1>

- 640 Nguyen, T., Janik, L., Raupach, M., 1991. Diffuse reflectance infrared fourier transform (DRIFT)  
641 spectroscopy in soil studies. *Soil Res.* 29, 49. <https://doi.org/10.1071/SR9910049>
- 642 Niu, H., Kinnunen, P., Sreenivasan, H., Adesanya, E., Illikainen, M., 2020. Structural collapse in  
643 phlogopite mica-rich mine tailings induced by mechanochemical treatment and implications  
644 to alkali activation potential. *Miner. Eng.* 151, 106331.  
645 <https://doi.org/10.1016/j.mineng.2020.106331>
- 646 NLK, 2002. Ecosmart concrete project: Metakaolin Pre-feasibility study, Report EA2860.  
647 Vancouver, British Columbia.
- 648 Novais, R.M., Ascensão, G., Tobaldi, D.M., Seabra, M.P., Labrincha, J.A., 2018. Biomass fly ash  
649 geopolymer monoliths for effective methylene blue removal from wastewaters. *J. Clean.*  
650 *Prod.* 171, 783–794.
- 651 O'Brien, H., Heilimo, E., Heino, P., 2015. Chapter 4.3 - The Archean Siilinjärvi Carbonatite  
652 Complex, in: Maier, W.D., Lahtinen, R., O'Brien, Hugh (Eds.), *Mineral Deposits of*  
653 *Finland*. Elsevier, pp. 327–343. <https://doi.org/10.1016/B978-0-12-410438-9.00013-3>
- 654 Oelkers, E.H., Gislason, S.R., 2001. The mechanism, rates and consequences of basaltic glass  
655 dissolution: I. An experimental study of the dissolution rates of basaltic glass as a function  
656 of aqueous Al, Si and oxalic acid concentration at 25°C and pH = 3 and 11. *Geochim.*  
657 *Cosmochim. Acta* 65, 3671–3681. [https://doi.org/10.1016/S0016-7037\(01\)00664-0](https://doi.org/10.1016/S0016-7037(01)00664-0)
- 658 Palomo, A., Glasser, F., 1992. Chemically-bonded cementitious materials based on metakaolin. *Br.*  
659 *Ceram. Trans. J.* 91, 107–112.
- 660 Panias, D., Giannopoulou, I.P., Perraki, T., 2007. Effect of synthesis parameters on the mechanical  
661 properties of fly ash-based geopolymers. *Colloids Surf. Physicochem. Eng. Asp.* 301, 246–  
662 254. <https://doi.org/10.1016/j.colsurfa.2006.12.064>
- 663 Passuello, A., Rodríguez, E.D., Hirt, E., Longhi, M., Bernal, S.A., Provis, J.L., Kirchheim, A.P.,  
664 2017. Evaluation of the potential improvement in the environmental footprint of  
665 geopolymers using waste-derived activators. *J. Clean. Prod.* 166, 680–689.  
666 <https://doi.org/10.1016/j.jclepro.2017.08.007>
- 667 Petrillo, A., Cioffi, R., De Felice, F., Colangelo, F., Borrelli, C., 2016. An environmental  
668 evaluation: A comparison between geopolymer and OPC concrete paving blocks  
669 manufacturing process in Italy. *Environ. Prog. Sustain. Energy* 35, 1699–1708.  
670 <https://doi.org/10.1002/ep.12421>
- 671 Provis, J., 2013. Alkali activated materials: state-of-the-art report, RILEM TC 224-AAM. Springer,  
672 New York.
- 673 Rattanasak, U., Chindaprasit, P., 2009. Influence of NaOH solution on the synthesis of fly ash  
674 geopolymer. *Miner. Eng.* 22, 1073–1078. <https://doi.org/10.1016/j.mineng.2009.03.022>
- 675 Rees, C.A., Provis, J.L., Lukey, G.C., van Deventer, J.S.J., 2007. In Situ ATR-FTIR Study of the  
676 Early Stages of Fly Ash Geopolymer Gel Formation. *Langmuir* 23, 9076–9082.  
677 <https://doi.org/10.1021/la701185g>
- 678 Rehman, I., Bonfield, W., 1997. Characterization of hydroxyapatite and carbonated apatite by photo  
679 acoustic FTIR spectroscopy. *J. Mater. Sci. Mater. Med.* 8, 1–4.  
680 <https://doi.org/10.1023/A:1018570213546>
- 681 Sagoe-Crentsil, K., Weng, L., 2006. Dissolution processes, hydrolysis and condensation reactions  
682 during geopolymer synthesis: Part II. High Si/Al ratio systems. *J. Mater. Sci.* 42, 3007–  
683 3014. <https://doi.org/10.1007/s10853-006-0818-9>
- 684 Schingaro, E., Lacalamita, M., Scordari, F., Mesto, E., 2013. 3T-phlogopite from Kasenyi  
685 kamafugite (SW Uganda): EPMA, XPS, FTIR, and SCXRD study. *Am. Mineral.* 98, 709–  
686 717. <https://doi.org/10.2138/am.2013.4283>
- 687 Slaty, F., Khoury, H., Rahier, H., Wastiels, J., 2015. Durability of alkali activated cement produced  
688 from kaolinitic clay. *Appl. Clay Sci.* 104, 229–237.  
689 <https://doi.org/10.1016/j.clay.2014.11.037>

- 690 Smith Aitken, W.W., 1965. An occurrence of phlogopite and its transformation to vermiculite by  
691 weathering. *Mineral. Mag. J. Mineral. Soc.* 35, 151–164.  
692 <https://doi.org/10.1180/minmag.1965.035.269.18>
- 693 Thinkstep, 2019. Description of the CML 2001 method [WWW Document]. URL [http://www.gabi-](http://www.gabi-software.com/support/gabi/gabi-lcia-documentation/cml-2001/)  
694 [software.com/support/gabi/gabi-lcia-documentation/cml-2001/](http://www.gabi-software.com/support/gabi/gabi-lcia-documentation/cml-2001/) (accessed 6.30.19).
- 695 Van Den Heede, P., De Belie, N., 2012. Environmental impact and life cycle assessment (LCA) of  
696 traditional and “green” concretes: Literature review and theoretical calculations. *Cem.*  
697 *Concr. Compos.* 34, 431–442. <https://doi.org/10.1016/j.cemconcomp.2012.01.004>
- 698 van Deventer, J.S.J., San Nicolas, R., Ismail, I., Bernal, S.A., Brice, D.G., Provis, J.L., 2015.  
699 Microstructure and durability of alkali-activated materials as key parameters for  
700 standardization. *J. Sustain. Cem.-Based Mater.* 4, 116–128.  
701 <https://doi.org/10.1080/21650373.2014.979265>
- 702 Veiderma, M., Knubovets, R., Tõnsuaadu, K., 1998. Structural properties of apatites from Finland  
703 studied by FTIR spectroscopy. *Bull. Geol. Soc. Finl.* 70, 69–75.  
704 <https://doi.org/10.17741/bgsf/70.1-2.005>
- 705 Vickers, L., van Riessen, A., Rickard, W.D.A., 2015. Fire-Resistant Geopolymers, SpringerBriefs  
706 in Materials. Springer Singapore, Singapore. <https://doi.org/10.1007/978-981-287-311-8>
- 707 Walkley, B., San Nicolas, R., Sani, M.-A., Rees, G.J., Hanna, J.V., van Deventer, J.S.J., Provis,  
708 J.L., 2016. Phase evolution of C-(N)-A-S-H/N-A-S-H gel blends investigated via alkali-  
709 activation of synthetic calcium aluminosilicate precursors. *Cem. Concr. Res.* 89, 120–135.  
710 <https://doi.org/10.1016/j.cemconres.2016.08.010>
- 711 Wei, B., Zhang, Y., Bao, S., 2017. Preparation of geopolymers from vanadium tailings by  
712 mechanical activation. *Constr. Build. Mater.* 145, 236–242.  
713 <https://doi.org/10.1016/j.conbuildmat.2017.03.234>
- 714 Ye, J., Zhang, W., Shi, D., 2014. Effect of elevated temperature on the properties of geopolymer  
715 synthesized from calcined ore-dressing tailing of bauxite and ground-granulated blast  
716 furnace slag. *Constr. Build. Mater.* 69, 41–48.  
717 <https://doi.org/10.1016/j.conbuildmat.2014.07.002>
- 718 N. Ye, J. Yang, X. Ke, J. Zhu, Y. Li, C. Xiang, H. Wang, L. Li, B. Xiao, Synthesis and  
719 Characterization of Geopolymer from Bayer Red Mud with Thermal Pre-treatment, *J. Am.*  
720 *Ceram. Soc.* 97 (2014) 1652–1660. doi:10.1111/jace.12840.
- 721 Yip, C.K., Lukey, G.C., van Deventer, J.S.J., 2005. The coexistence of geopolymeric gel and  
722 calcium silicate hydrate at the early stage of alkaline activation. *Cem. Concr. Res.* 35, 1688–  
723 1697. <https://doi.org/10.1016/j.cemconres.2004.10.042>
- 724 Zhang, L., 2013. Production of bricks from waste materials – A review. *Constr. Build. Mater.* 47,  
725 643–655. <https://doi.org/10.1016/j.conbuildmat.2013.05.043>